Dual-functionalized titanium by ultrafast laser texturing to enhance human gingival fibroblasts adhesion and minimize Porphyromonas gingivalis colonization

Steve Papa, Alain Abou Khalil, Hind Hamzeh-Cognasse, Mireille Thomas, Mathieu Maalouf, Yoan Di Maio, Xxx Sedao, Alain Guignandon, Virginie Dumas

Applied Surface Science 606 (2022) 154784

Contents lists available at ScienceDirect

Applied Surface Science

journal homepage: www.elsevier.com/locate/apsusc

Full Length Article

Dual-functionalized titanium by ultrafast laser texturing to enhance human gingival fibroblasts adhesion and minimize *Porphyromonas gingivalis* colonization

Steve Papa [a,*], Alain Abou Khalil [b], Hind Hamzeh-Cognasse [a], Mireille Thomas [a], Mathieu Maalouf [a], Yoan Di Maio [c], Xxx Sedao [b,c], Alain Guignandon [a,1], Virginie Dumas [d,1]

[a] INSERM, U1059-SAINBIOSE, University of Lyon, Jean Monnet University, F-42270 Saint Priest en Jarez, France
[b] Laboratory Hubert Curien, UMR 5516 CNRS, Jean Monnet University, University of Lyon, F-42000 Saint-Etienne, France
[c] GIE Manutech-USD, 20 rue Benoît Lauras, F-42000 Saint-Etienne, France
[d] Laboratory of Tribology and Systems Dynamics, UMR 5513 CNRS, University of Lyon, National School of Engineers of Saint-Etienne, Lyon Central School, F-42100 Saint-Etienne, France

ARTICLE INFO

Keywords:
Laser-Induced Periodic Surface Structures
Femtosecond laser
Cell adhesion
Antibacterial surfaces
Gingival fibroblasts

ABSTRACT

Dental implant failure is primarily due to peri-implantitis, a consequence of bacterial penetration causing implant loosening. Beyond supporting the implant, the adhesion of gingival tissues to the surface is essential for its role as a physical barrier to bacteria. Surface nanotextures are widely known to affect wettability, protein adsorption, and cellular and/or bacterial adhesion. In this report, a femtosecond laser (fs-L) was used to design Laser-Induced Periodic Surface Structures (LIPSS) with Infra-Red (IR) or Green lasers on Ti6Al4V. Surface morphology, topography and wettability were characterized. Gingival fibroblasts adhesion was evaluated with sclerometer scratch tests and confirmed by ultrasonic bath cell detachment method. The fs-L texturing increases human gingival cells adhesion compared to polished surface. The adhesion of peri-implantitis associated bacteria was quantified. After 48 h of contact, IR LIPSS show antiadhesive properties for *Porphyromonas gingivalis*, whereas Green LIPSS, thanks to its smaller spatial period, have limited both *Streptococcus mutans* and *Porphyromonas gingivalis* adhesion. Thus, LIPSS generated on Ti6Al4V surfaces, especially Green LIPSS, are identified as having double biological functionality: repellent for bacteria and adhesive for gingival tissues. This study proves that fs-L processing is an innovative tool with potential to enhance implant success paving the way towards dual functionality.

1. Introduction

Titanium and its alloys, such as *Titanium-6Aluminum-4Vanadium* (Ti6Al4V), have been used as the main biomaterial for dental implant devices due to its excellent physico-chemical properties and high biocompatibility with host tissues [1,2]. Osseointegrated dental implants are safe and present high survival rates at about 90% and minimal marginal bone resorption in the 10 years following implantation [3]. Nevertheless, once exposed to the oral environment implants are subject to oral microbial adhesion and biofilm formation, resulting in peri-implantitis: one of the most important biological complications in recent implantology, that remains unsolved [4,5]. Peri-implantitis is a destructive inflammatory lesion that affects the surrounding soft and hard tissues with loss of supporting bone [3]. A recent review reports that peri-implantitis affects up to 47% of failed oral implants [6].

In transmucosal implants, bacterial infection leading to biofilm formation is due to bacterial penetration through the soft tissues coming in contact with the implant surface. Indeed, the weak point of dental implants is the passage of bacteria from the oral cavity into the bone tissues [7]. If there is an imperfect gingival adhesion to the implant surface, rapid infiltration of oral microbes is possible and may lead to gingival inflammation and recession, causing bone resorption and finally implant failure. Thus, the creation of a biological barrier with adhesive peri-implant soft tissues is a crucial point to avoid peri-implantitis and

* Corresponding author at: INSERM, U1059-SAINBIOSE, University of Lyon, Jean Monnet University, F-42270 Saint Priest en Jarez, France
E-mail address: steve.papa@univ-st-etienne.fr (S. Papa).
[1] These authors share senior authorship.

https://doi.org/10.1016/j.apsusc.2022.154784
Received 28 June 2022; Received in revised form 31 August 2022; Accepted 2 September 2022
Available online 7 September 2022

preserve dental implants. Implants that can perform dual functions, appropriately named "*duel*" surfaces recently by Damiati [8], such as enhancing cell adhesion and activity, and reducing bacterial adhesion, would help to improve the outcomes of dental surgeries. These implants are of particular importance considering an ever increasing risk of infection as bacteria gain resistance to antibiotics [9].

Innovative surfaces have been developed based on the idea of modifying adhesion strength between bacterial or mammalian cells and a substrate, achieved by tailoring the surface nanostructures [10–12]. Amongst several surface treatments, ultrashort pulse lasers texturing has emerged as a powerful and versatile surface engineering process to limit biofilm formation on implant surfaces [13,14]. Surface topographic features may significantly modify the properties of surfaces that allow or limit cell and/or bacteria adhesion [15–17]. Femtosecond laser (fs-L) allows for the creation of diverse types of laser-induced surface nanostructures, such as laser-induced periodic surface structures (LIPSS) with different periodicities [18,19]. The fs-L treatment is a highly valid innovative approach due to its simplicity which does not require clean room facilities and is possible to perform in air environments. Therefore, it is a suitable candidate for implementation in an industrial context of dental implants processing.

Following surgery, gingival fibroblasts, the major cellular component in the peri-implant connective tissue layer, start to proliferate, repopulate, and generate an extracellular matrix (fibronectin, collagen) at the transmucosal region that adheres on the implant surfaces. Thus, in this study, we evaluated the adhesion of a 3-week culture of human gingival fibroblasts with a large amount of extracellular matrix on nanotextured titanium. Two mechanical detachment evaluation devices were used: a sclerometer and an ultrasonic bath.

The pathogenesis of periodontal inflammation begins with the colonization by pathogenic bacteria. According to Socransky [20], specific bacteria have niche locations of colonization within the oral cavity, and their characteristics are subdivided into primary and secondary colonizers. We have included *Streptococcus mutans* in our study because *Streptococci* are the dominating bacteria at peri-implant tissue interface within the first 48 h following implantation[21]; and *Porphyromonas gingivalis*, a secondary colonizer, for its strong association with peri-implantation pathologies, as a member of the red complex, responsible of implant failure [22,23].

Surface engineering-based approaches are being considered as a highly competitive alternative to obtain comparable performance for delivering adhesive and repellent factors more safely and efficiently. When we consider the upper part of a dental implant, we can assume that perfectly flat medical titanium is offering a fair defense to infection. Mirror polished titanium is known to offer a good resistance to bacterial biofilm formation and development, nevertheless this flat surface is not able to sustain 3D tissue adhesion. The adhesion of the gingival tissues to the implant surface is essential for its role as a physical barrier to bacteria. However, this seal is often obtained only by the physical adaptation of the mucosa, rather than a biological attachment onto the implant surface [24,25]. One solution is to increase the roughness of the implant surface to increase surface area for cell adhesion. However, this roughness might also promote the adhesion of other cells such as microbial pathogens. Just like for eukaryotic cells, bacteria adhesion is enhanced on rough surfaces as opposed to polished ones. Therefore, a compromise must be found by increasing surface roughness to promote fibroblasts adhesion, but at a nanometer scale in order to limit bacterial attachment by reducing its contact area to the surface [26].

So, the aim of the present study is to evaluate the adhesion strength of a fibroblast cell layer on two different laser textured surfaces and investigate the initial bacterial adherence. Two types of LIPSS are presented in this study, nanostructures made with infra-red Laser (IR LIPSS) and nanostructures made with green Laser (Green LIPSS); both characterized for topography (Sa; Sdr; Str; ripples density, period and depth) and wettability parameters. The novelty of this study is the evaluation of both human gingival fibroblast and peri-implantitis associated bacteria (*S. mutans* and *P. gingivalis*) on fs-L textured titanium surface. Moreover, this work allowed to identify dual-functionalized titanium by ultrafast laser texturing, to enhance human gingival fibroblasts adhesion and minimize bacterial colonization, which is of primary interest for dental implant applications.

2. Material and methods

Mirror polished titanium alloy samples of Ti6Al4V were purchased from Goodfellow (Huntingdon, UK). The Ti6Al4V samples were dimensioned in squares with a surface area measuring 1 cm^2, and a thickness of 1 mm by the supplier prior to the shipment.

2.1. Femtosecond laser irradiation

Titanium samples were textured using a Tangor HP fs-L from Amplitude Systems (France) and a Galvo scanner (Scanlab, Germany) at GIE Manutech-USD platform. The fs-L used emits at a central wavelength of 1030 nm and a pulse duration of around ~400 fs. The laser beam was linearly polarized. All the samples were placed on 3D-XYZ translation stages from Aerotech (Bavaria, Germany). Scanlab GmbH's intelliSCAN 14 scanner was finally associated with 2 different f-theta lenses of 88 mm and 100 mm depending on the wavelength used. IR LIPSS were generated on titanium alloy surfaces at 1030 nm wavelength using a 100 mm f-theta lens. The second harmonic generation of the Tangor laser, i.e. 515 nm green wavelength, was achieved through a set of non-linear crystals and used to create Green LIPSS on titanium surface samples with a 88 mm f-theta to focus the beam on the sample. Laser parameters used are detailed in Table 1.

The peak fluence is defined as: $F_{peak} = 2\,E/(\pi\,\omega_0^2)$, where E is the pulse energy and ω_0 is the radius of the focused beam. The full surface of the titanium samples was covered by IR or Green LIPSS for wettability and cell adhesion tests. For bacterial adhesion tests, laser textures were distributed in 4000 μm × 100 μm bands alternating with 100 μm of untextured mirror-polished titanium to get a local control.

2.2. Surface morphology

Scanning Electron Microscopy (SEM) was used to visualize and characterize the different laser induced patterns. A Tescan VEGA3 SB, Brno Czech Republic electron microscope was used operating at 20 kV and using the secondary electron detector.

2.3. Surface topography

Atomic Force Microscopy (AFM, JPK Instruments, Berlin, Germany) was used to characterize the different nanostructures in tapping mode in air with an adapted probe (NanoWorld Arrow-NCR) to avoid impact over surface topography representation. Measurements were realized in a perpendicular way to the LIPSS to give the best surface topography visualization. Data topographies were analyzed with Mountains Map® 8.2 software. Surface roughness parameters are computed on the treated surfaces and this study focuses on:

- Ripples (LIPSS) density calculated as cm/cm^2;

Table 1
Laser parameters used to create IR and Green LIPSS.

LIPSS	Pulse Energy	Peak Fluence	Distance between pulses (Δx)	Hatching (Δy)	F-theta
IR	1.07 μJ	$F_{peak} = 0.26$ J/cm2	5 μm	5 μm	100 mm
Green	0.55 μJ	$F_{peak} = 0.18$ J/cm2	5 μm	5 μm	88 mm

- Areal arithmetic mean height Sa (nm) which expresses the difference in height of each point compared to the arithmetical mean of the surface. This parameter is used to evaluate surface roughness.
- Sdr (Developed interfacial area ratio) which expresses the ratio between the area of the "real" developed surface and the area of the "projected" surface
- Average spatial period and depth of the ripples.
- Texture aspect ratio Str which expresses the isotropy and anisotropy of the topography. Str is a value from 0 to 1. A value close to 0 indicates directionality (anisotropy) while a value close to 1 indicates that the surface does not exhibit preferred directions (isotropy).

Definitions of surface parameters are stated by ISO 25178 standards.

2.4. Wettability

Wettability measurements were carried out with a laboratory-developed multiscale and multifunctional system within the MANUTECH-USD consortium. They were performed in a controlled atmosphere (Temperature (T) = 23.1 ± 0.85 °C, Relative humidity (RH) = 44 ± 6.5 %), 24 h after a sterilization procedure, in which the samples received an ultrasonication cleaning (Triton 3% in demineralized water for 15 min then only demineralized water for 15 min) and an autoclaving treatment at 134 °C for 19 min. The data represents the measurements from 4 consecutive, independent and contact-less droplets on each surface. 3 μL droplets of water were deposited on the surfaces, and the evolution of the droplet shape was visualized with a camera and a sample rotation stage enabling 360° contact angle measurements. The platform moved at a speed of 0.1 rad.s^{-1}. The droplet profile and especially the contact angle (CA) were extracted from the complete droplet 360° rotation leading to approximately 80 measurements per droplet.

2.5. Cell culture

Human Gingival Fibroblasts (HGnF) from Cliniscience at passage 6 were maintained in a T75-flask until 70% confluency in culture medium (ScienCell l2301-SC). Cells were then seeded on Ti6Al4V samples at 15,000 cells/cm^2 in 24-well plates with culture medium. At 24 h post-seeding, samples were moved to another well with fresh medium. Thereafter, the culture medium was renewed every 4 days for 3 weeks; the last medium being renewed 7 days before adhesion tests at 3 weeks, to avoid the risk of cell layer detachment during medium change, especially on polished samples.

2.6. Cell adhesion tests

Fresh living 3 weeks fibroblasts cultures were used in both adhesion tests.

Scratch test: a sclerometer (Multi Function Tribometer MFT-5000 RTEC instruments) with an indenter (angle 120°, radius 200 μm) was used to scratch the 3 weeks cell layer with a 0.2 N load over 5 mm at a speed of 0.167 mm/s. Two scratches were realized on each sample and after samples were immersed in 10% Formalin (Sigma HT501128) for 15 min RT right after the scratch process to fix the tissue-like, then conserved in phosphate-buffered saline (PBS) 4 °C until staining and observation.

Ultrasonic (US) bath test: 3 weeks cell layer was stained with methylene blue for 30 s RT to facilitate tissue-like detachment observation. Then samples were rinsed in PBS and put in PBS in a beaker, placed in the US bath (Velleman VTUSC2) with a power of 70 W and a frequency of 50 Hz. Cycle lasting 15 s were realized successively until full tissue-like detachment.

2.7. Bacterial strains and culture conditions

Streptococcus mutans ATCC 25175 strain was isolated on brain–heart infusion (BHI) agar plates and grown in a BHI broth. 2 mL of 4 h broth (obtained from a 24 h broth) diluted to 1. 10e8 UFC/mL were incubated over titanium samples for 48 h at 37 °C under agitation (160–180 rpm).

Porphyromonas gingivalis ATCC 33277 strain was isolated on Columbia agar with 5% of sheep blood under anaerobic conditions using the Genbox system (Biomerieux); then cultured 4 days in Schaedler broth with 650 μL of mineral oil (Sigma M5904) at a ratio of 1:20 (mineral oil: medium). 1 mL of broth was incubated over titanium samples for 48 h at 37 °C under anaerobic conditions.

For both bacteria, after 48 h of incubation, media were removed; bacteria were fixed with formalin 10% (Sigma HT501128) for 40 min at RT; washed with PBS and kept in PBS at 4 °C until staining.

2.8. Fluorescent cell and bacteria labeling

Scratched and fixed samples were permeabilized with 0.1% Triton X-100 in PBS for 3 min RT. Samples were incubated with rhodamine-conjugated phalloidin diluted at 1:50 in PBS at 37 °C for 1.5 h for f-actin labeling. Nuclei labeling was performed with 1 μg/ml DAPI (4′,6-diamidino-2-phénylindole) diluted at 1:100 in PBS at 37 °C for 20 min. Cells were incubated with primary fibronectin antibodies (Sigma; F3648), diluted at 1:100 in PBS, at 37 °C for 2 h. Then, the samples were incubated with secondary 488 conjugated fluoprobes diluted at 1:250 in PBS, for 1h30 at room temperature. Washes were performed using PBS between each step. Fixed bacteria were stained with calcein AM (Invitrogen; C3099) at 10 μg.mL-1 for 20 min at 37 °C.

2.9. Image acquisition and analysis

Fixed bacteria were dehydrated in graded ethanol solutions (70, 80, 90 and 100%) air-dried at RT and analyzed with SEM at 5 kV with a secondary electron detector. Fluorescent microscopy (ZEISS LSM 800 Airyscan, Oberkochen, Germany) was used to image stained bacterial samples (10x10 mm tiles); and stained cells scratched areas (6x3 mm tiles). Smartphone (Xiaomi mi11) was used to image US bath cycles (every 15 s from T0s to full detachment). Cell adhesion images analysis was performed with GIMP (2.10.30) to increase torn off (scratch test) or attached (ultrasonic bath) areas contrast; and ImageJ to threshold and measure those areas. Bacterial images analysis was performed with ImageJ by measuring mean fluorescence in 45 areas (51 mm^2) per condition and making a percent ratio with local polished control.

2.10. Statistical analysis

All statistical analyses were performed using GraphPad Prism 8 software. Wettability and scratch tests box plots represent mean, quartiles and min/max value; statistical analyses were performed using Mann-Whitney *U* test. Bacterial data are presented as mean ± SEM, statistical analyses were performed using *t*-test.

3. Results

The fs-L irradiation of Ti6Al4V at two wavelengths with linear polarization creates highly ordered/periodic texturing called IR LIPSS and Green LIPSS as presented on SEM images in Fig. 1A. The AFM measurement enables a 3D-view reconstruction of the surface topography presented in Fig. 1B and the calculation of different surface parameters using MountainsMap® software compiled in Fig. 1C. As seen in the SEM images, it is confirmed that the furrows created on textured surfaces have a density twice more important on Green LIPSS (44 239 cm/cm^2) than on IR LIPSS (22 309 cm/cm). This important density of furrows increases surface complexity (Sdr) of IR LIPSS (33.11 %) and Green LIPSS (29.81 %), in comparison with polished surfaces (0.11 %).

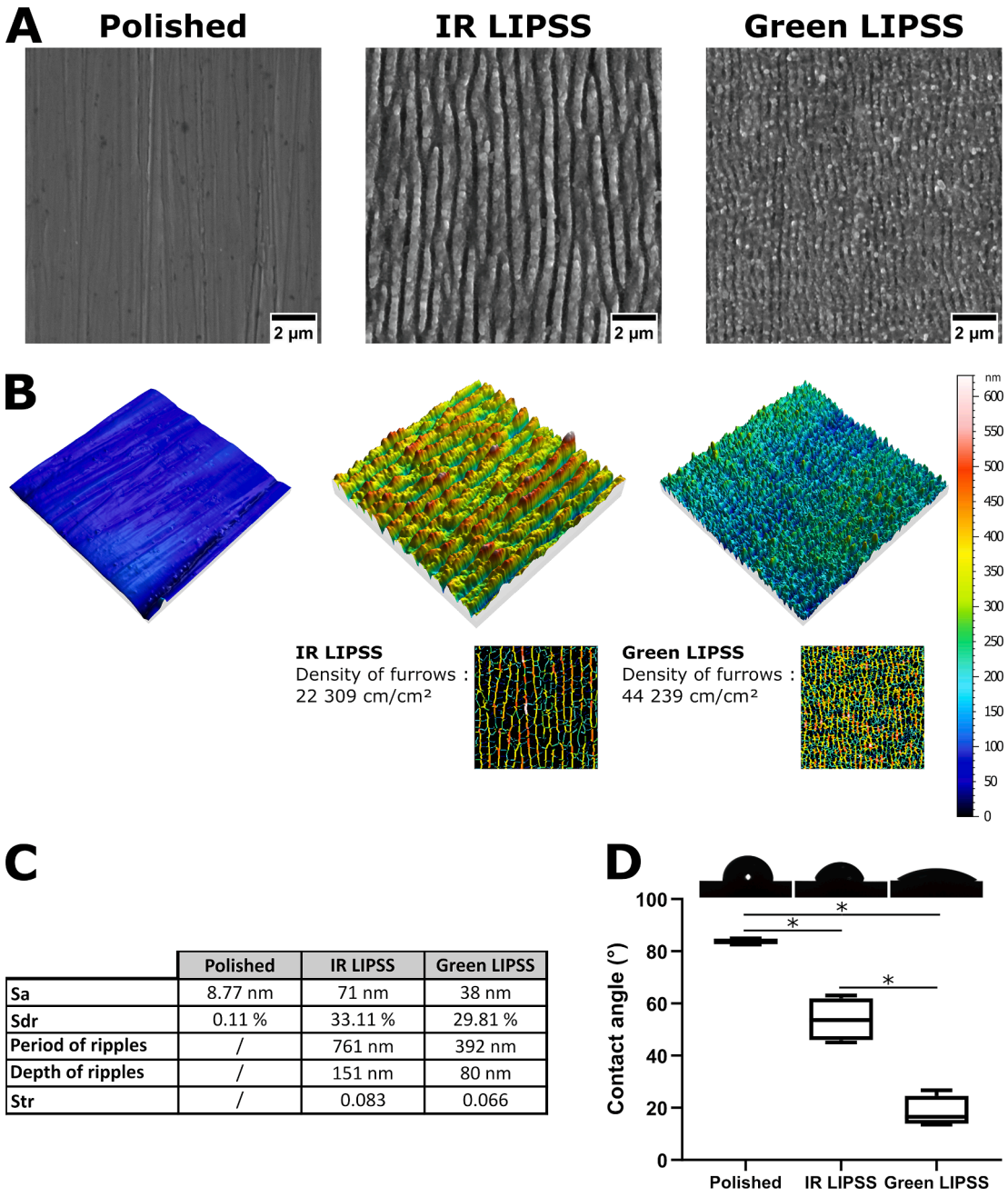

	Polished	IR LIPSS	Green LIPSS
Sa	8.77 nm	71 nm	38 nm
Sdr	0.11 %	33.11 %	29.81 %
Period of ripples	/	761 nm	392 nm
Depth of ripples	/	151 nm	80 nm
Str	/	0.083	0.066

Fig. 1. Surfaces characterization. **A.** SEM images of polished, IR LIPSS and Green LIPSS surface. **B.** 3D images and representative images of ripples density from AFM measurements of polished, IR LIPSS and Green LIPSS surfaces. **C.** Surface parameters table including areal arithmetic mean height (Sa), developed interfacial area ratio (Sdr) and texture aspect ratio (Str). **D.** Sessile drop contact angle over sterilized polished, IR LIPSS and Green LIPSS surfaces. Contact angles of the drops are measured on a 360° rotation and presented as a box plot. Bottom and top bars stand for minimum and maximum concentrations. n = 4; Mann-Whitney *U* test; * p = 0.0286.

Rugosity (Sa) on IR LIPSS (71 nm) is approximately 2 times higher than on Green LIPSS (38 nm). For spatial period and depth of both LIPSS, there is an almost 2 times factor between IR LIPSS (761 nm / 151 nm) and Green LIPSS (392 nm / 80 nm) knowing that the laser wavelength is divided by 2. The Str that is near 0 in both IR and Green LIPSS (0.083 / 0.066) indicates the anisotropy of those two surfaces. Finally, the results of contact angle measurements on sterilized surfaces presented in Fig. 1D, show the significant decrease of contact angle due to the presence of ripples on surfaces correlated to an increase in the wettability which is significantly higher with the presence of Green LIPSS compared to IR LIPSS.

Fig. 2A presents the sclerometer process used for scratch tests over the 3 weeks cultivated living fibroblasts layer, used to obtain scratches presented in Fig. 2B and quantified in Fig. 2C. Torn off area of the cell layer is visually and quantitatively higher on control polished surfaces (up to 5.8 mm^2) compared to textured ones (close to 0 mm^2, limited to indenter passage), with no significant difference between IR and Green LIPSS. This result confirms an increase of fibroblasts adhesion allowed by the presence of LIPSS on Ti6Al4V surfaces.

Fig. 3A presents the process used for ultrasonic bath tests over the 3 weeks cultivated living fibroblasts layer, stained with methylene blue to facilitate the visualization of cell layer detachment. Fig. 3B shows the images of gingival tissue-like on every surface at two time points (0 s and 30 s) of the US bath test. The evolution of the percent of covered area is

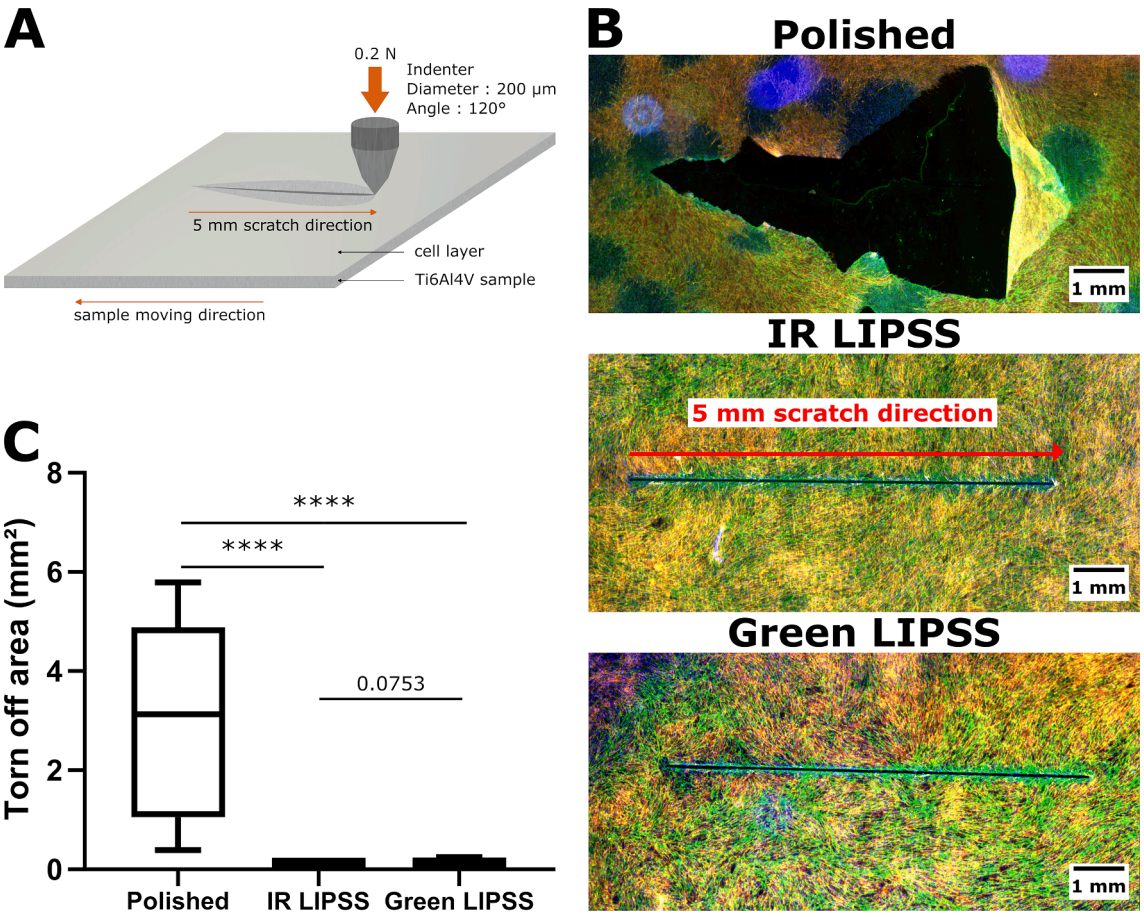

Fig. 2. Scratch tests to evaluate fibroblasts adhesion on the different surfaces. **A.** Schematic of scratch test realized with a sclerometer on living fibroblasts culture. **B.** Representative merged fluorescence images (red: cytoskeleton; blue: nucleus; green: fibronectin) of torn off fibroblastic layer after sclerometer scratch 3 weeks post seeding on polished, IR LIPSS or Green LIPSS samples. **C.** Graph represents the torn off area (mm^2) as a box plot. Bottom and top bars stand for minimum and maximum concentrations. n = 19 scratches/group; Mann-Whitney *U* test; **** $p < 0.0001$.

shown over time for every surface in Fig. 3C. The time for mean detachment of 50% of the cell layer is presented as well. It takes at least twice the amount of time to remove half of the cell layer on Green LIPSS (40.2 s) and IR LIPSS (52 s) compared to control polished surface (19.7 s).

Both tested bacterial strains are presented over textured surfaces through SEM images in Fig. 4A; showing that IR LIPSS spatial period exhibit roughly the same dimensions of *S. mutans* whereas Green LIPSS are smaller than the size of this bacterium; and that both IR and Green LIPSS are smaller than *P. gingivalis* size. Imaging of stained bacteria after 48 h of cultured on partially textured samples (Fig. 4B), allowed for the quantification of bacterial adhesion over LIPSS with a ratio compared to adjacent control on bordering polished surfaces. Results presented in Fig. 4C showing a decrease of *S. mutans* adhesion on Green LIPSS by 4% compared to polished-control surfaces, and 7% compared to IR LIPSS. Whereas *P. gingivalis* adhesion is decreased respectively by 21% and 30% over IR and Green LIPSS compared to the polished-control.

4. Discussion

In the present study, we show that nanostructures produced by fs-L, also called LIPSS, are able to significantly improve gingival tissue-like adhesion, while limiting the adhesion of two oral bacteria involved in peri-implantitis.

Within minutes of implant surgery, proteins from saliva start to adhere on the implant surface and it is known that hydrophilic surfaces improve protein adsorption and therefore cell adhesion. Contact angle testing can approximate how well a cell could adhere to a surface [27–29].

The LIPSS of our study generated with an IR or Green Laser are more hydrophilic than polished titanium-based surfaces. The link between fs-L induced topography and Ti6Al4V surface wettability agrees with previous studies, showing that surface texturing can increase hydrophilicity [29]. However, according to Kietzig [30], wettability change of metallic surfaces, induced by ultrafast laser texturing is not only due to topographic changes, but is also related to surface chemistry changes. To complete the characterization of the impact of LIPSS on cell adhesion, it would be interesting in the future to study the surface chemistry of Ti6Al4V samples to identify oxides known to form during fs-L texturing [31]. To this end, a combination of FIB-STEM [32], TOF-SIMS [33], RAMAN and XPS may be pursued to evaluate the oxide layer thickness, oxides composition and the adsorption at the oxidized surface. Nevertheless, the increased wettability is of interest for the adhesion of fibroblasts, as cells that properly adhere to a surface cover a wider area (by spreading or migration) and typically with considerable strength. Adhesion strength assays quantify how cells stay attached when a detachment force is added. These assays can range from analyzing the forces on a single cell to a population of cells. In the literature the methods generally used, tend to observe cell adhesion at the individual scale, such as staining focal contacts [34,35], a method more qualitative than quantitative, or micromanipulation with AFM [36] measuring the forces acting on a single cell. Few methods are available at the tissue or cell layer scale. Only new methods are being created combining AFM and other tools and techniques, but it requires specific and expensive

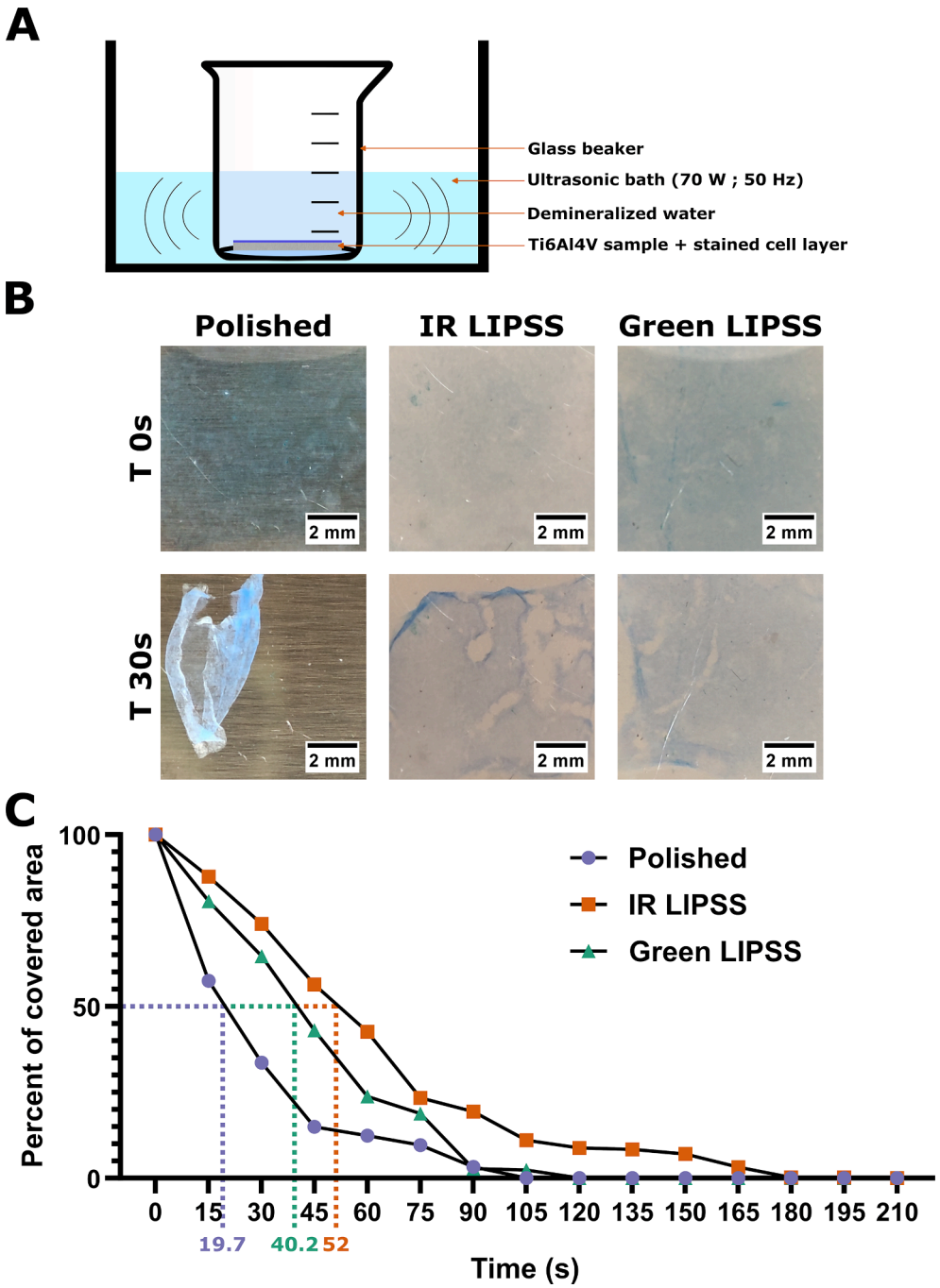

Fig. 3. Ultrasonic bath to evaluate fibroblasts adhesion on the different surfaces. **A.** Schematic of ultrasonic bath test realized on methylene blue stained living fibroblasts culture. **B.** Representative images of fibroblasts layers on polished, IR LIPSS and Green LIPSS samples before (T 0 s) and after 2 cycles (T 30 s) of ultrasonic bath. **C.** Graph presents the percentage of covered area over time as mean (n = 5); time for mean 50% of detachment is represented over x axis.

equipment [37]. There are other techniques, simpler to implement, but not fully accurate, such as the flow technique or the use of a centrifuge. Hydrodynamic shear assays and rotating disks are other methods but require specific cells and/or conditions (short term adhesion) [38,39]. In our study, a mechanical strategy using a sclerometer was developed to measure tissue-like adhesion on polished or nanotextured titanium surfaces, during a dynamic scratch test. The sclerometer method starts from the principle conventionally used in the industry to measure the adhesion of coatings. In an innovative way, we have diverted this method to apply it to the measurement of a cell layer adhesion. The results of this new method were confirmed by the ultrasonic bath cell detachment, generally used for cleaning surfaces, but the imaging over time of tissue detachment proved to be very accurate to measure the adhesion of the tissue-like (time to detach 50% of the tissue). The use of fs-L texturing to improve cell adhesion on a surface have been studied on surfaces such as PET with imaging approach [40]. Here it is confirmed on titanium with methods closer to physiological and clinical context (scratch and ultrasonic bath tests); which is promising for dental implant applications. Sclerometer scratch tests presented in this study could be proposed as a new pre-clinical test to evaluate the performance of the surfaces of future dental implants. Indeed, in the context where lifespan of the implants is compromised by poor adhesion of gingival tissue to the Ti6Al4V surface, new tests are needed for the industrial level to quantitatively assess gingival tissue adhesion.

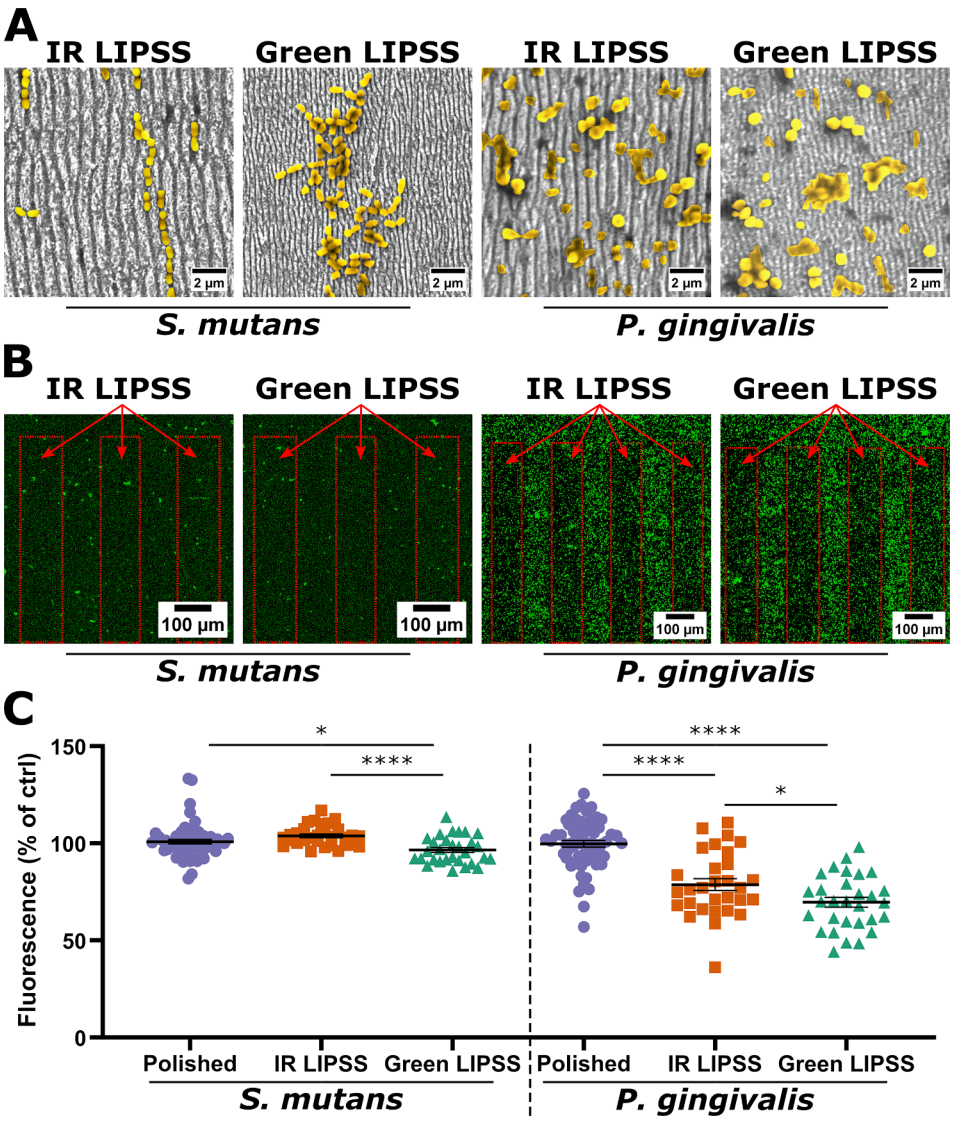

Fig. 4. Evaluation of *S. mutans* and *P. gingivalis* adhesion on the different surfaces. **A.** SEM images of *S. mutans* and *P. gingivalis* on IR LIPSS or Green LIPSS surfaces, bordered with adjacent polished surfaces. **B.** Representative fluorescence images of calcein-stained *S. mutans* and *P. gingivalis* 48 h post seeding on samples. **C.** Graph presenting the fluorescence quantification as mean ± SEM. n = 45 area/group; *t*-test; *p = 0.024; ****p < 0.0001.

LIPSS attract lots of attention for implant surface improvement because it is a nanoscale topography, which can be simply generated on titanium alloys by a single-pass laser beam irradiation [18]. The presented results show that laser processing increased surface roughness and, in turn, the area available for fibroblast layer adhesion. On the other hand, the periodicity of ripples can be controlled and reduced by changing the laser wavelength in order to minimize the contact area between the surface and bacteria [41]. Laser processing is able to generate regular and precise nanostructures which lead to antibacterial properties [11,12]. Roughness is a measure of amplitude with no spatial information, so it needs to be paired with other surface parameters [42]. Therefore, it is important to identify nanostructures that can be repellent to bacteria. If we consider bacteria repellence by mechanical inhibition, it is clear that the contact surface between bacteria and the topography must be reduced. The correlation between biofilm organization and surface topography is consistent with a study from Epperlein [11] showing the antibacterial properties of IR LIPSS against bacteria larger than the topography spatial period. This point is definitely of major interest to avoid bacterial adhesion on a surface. So, it seems it is better to obtain a pattern with a spatial period lower than the bacteria diameter. The IR LIPSS spatial period is 760 nm while the Green LIPSS is 390 nm whereas the diameters of the two bacteria studied are about 500 nm to 1 µm. From the SEM images, it is clearly seen that some *streptococci* can be mechanically retained in the valleys of IR LIPSS with the larger periodicity, due to their "*double cocci*" shape and their organization in chains. This retention in the valleys should be avoided as it could lead to the rapid development of a biofilm and difficulties in the implant cleaning. Bacterial adhesion evaluations of both strains, added to the size ratio between LIPSS and bacteria, underline the importance of reducing the area of contact between a single bacterium and the surface to reduce bacterial adhesion on surfaces such as Ti6Al4V. Our results confirm the findings of Linklater concerning the manufacturing of a "*mechano-bactericidal surface pattern*" [43]. One of our perspectives would be to use a fs-L with a lower wavelength, in particular at UV wavelength, in order to obtain LIPSS with smaller periodicity (around 200 nm) [44]. To go further than limiting bacterial adhesion, it is known that some bioinspired nanopillar structures can have a bactericidal effect. Density, spatial period and depth of ripples could be correlated with the "*fakir effect*" on the bacterium (like the bacterium is laying on a bed of nails) that disrupts membrane and thus proliferation [45]. For instance, nanopillars with a size of 60–215 nm and spaced out 100–380 nm, create a "mechanical bactericidal mechanism" that ruptures or

deforms bacterial cell membranes [18,43]. An important note is that this was achieved on a polymer surface, not a titanium-based one. In the present study, IR LIPSS decrease *P. gingivalis* adhesion (21% decrease) whereas Green LIPSS, thanks to its smaller spatial period, have shown antiadhesive properties for both *S. mutans* (4% decrease) and *P. gingivalis* (30% decrease); compared to polished surfaces. So, future works will assess different laser processing parameters in order to generate surface morphologies able to increase the efficiency of the anti-bacterial effect, or even better, obtain a bactericidal effect with nanospikes with a high height/width ratio. Even if this remains a challenge for fs-L texturing on titanium, this application of fs-L is really promising in terms of surface functionalization [46]. Regarding our results, Green LIPSS is probably the better candidate, presenting a rugosity that increases gingival tissue-like adhesion with an antiadhesive functionalization regarding both of our peri-implantitis associated bacteria.

5. Conclusions

Laser processing is able to generate reproducible nano-textures (LIPSS) on a titanium-based surface in a single-step process. The results presented show that the LIPSS according to their morphologies can render a dual functionality to the titanium-based surface of dental implants. The two types of LIPSS, IR and Green, allow better adhesion of human gingival fibroblasts on a long-term culture. Moreover, the LIPSS can also reduce the adhesion of *P. gingivalis* with better efficiency for Green LIPSS over IR LIPSS. Considering the results of this study, LIPSS might feature considerable potential for transgingival parts of dental implants, facilitating the attachment of soft tissue and inhibiting the adhesion of bacteria. Further investigations are needed to explore the *in vivo* and clinical implications.

Funding

This project was funded by the European Commission LaserImplant project, grant agreement number: 951730. This work has been funded by a public grant from the French National Research Agency (ANR) under the Investments for the Future Program (PIA), which has the reference EUR MANUTECH SLEIGHT - ANR-17-EURE-0026.

CRediT authorship contribution statement

Steve Papa: Methodology, Validation, Formal analysis, Investigation, Writing – original draft, Writing – review & editing, Visualization. **Alain Abou Khalil:** Validation, Resources, Writing – review & editing. **Hind Hamzeh-Cognasse:** Conceptualization, Writing – review & editing. **Mireille Thomas:** Investigation, Resources, Writing – review & editing. **Mathieu Maalouf:** Writing – original draft, Writing – review & editing. **Yoan Di Maio:** Resources, Writing – review & editing. **Xxx Sedao:** Methodology, Validation, Resources, Writing – review & editing, Visualization, Supervision, Funding acquisition. **Alain Guignandon:** Conceptualization, Methodology, Writing – review & editing, Visualization, Supervision, Project administration, Funding acquisition. **Virginie Dumas:** Conceptualization, Methodology, Writing – original draft, Visualization, Supervision, Project administration, Funding acquisition.

Declaration of Competing Interest

The authors declare the following financial interests/personal relationships which may be considered as potential competing interests: Steve PAPA reports financial support was provided by French National Research Agency (ANR) - EUR MANUTECH SLEIGHT - ANR-17-EURE-0026. Xxx Sedao reports financial support was provided by European Commission LaserImplant project, grant agreement number 951730.

Acknowledgement

The authors thank Marie-Ange Eyraud for help with bacterial tests and Sylvie Peyroche for help with cell culture. Also thanks to Maryane Jacquier (SEM) and Claudie Petit (AFM) for help with microscopy acquisitions; finally thanks to Alina Hamri for help with wettability measurements and Ashlyn Hicks for the proofreading.

References

[1] S. Spriano, S. Yamaguchi, F. Baino, S. Ferraris, A critical review of multifunctional titanium surfaces: New frontiers for improving osseointegration and host response, avoiding bacteria contamination, Acta Biomater. 79 (2018) 1–22, https://doi.org/10.1016/j.actbio.2018.08.013.

[2] S. Ferraris, A. Cochis, M. Cazzola, M. Tortello, A. Scalia, S. Spriano, L. Rimondini, Cytocompatible and Anti-bacterial Adhesion Nanotextured Titanium Oxide Layer on Titanium Surfaces for Dental and Orthopedic Implants, Front. Bioeng. Biotechnol. 7 (2019) 103, https://doi.org/10.3389/fbioe.2019.00103.

[3] V. Moraschini, L.A.d.C. Poubel, V.F. Ferreira, E.D.S.P. Barboza, Evaluation of survival and success rates of dental implants reported in longitudinal studies with a follow-up period of at least 10 years: a systematic review, Int. J. Oral Maxillofac. Surg. 44 (3) (2015) 377–388, https://doi.org/10.1016/j.ijom.2014.10.023.

[4] F. Schwarz, J. Derks, A. Monje, H.-L. Wang, Peri-implantitis, J. Periodontol. 89 (2018) S267–S290, https://doi.org/10.1002/JPER.16-0350.

[5] C.R. Arciola, D. Campoccia, L. Montanaro, Implant infections: adhesion, biofilm formation and immune evasion, Nat. Rev. Microbiol. 16 (7) (2018) 397–409, https://doi.org/10.1038/s41579-018-0019-y.

[6] A. Shatta, S. Anil, Peri-Implantitis Revisited, IntechOpen (2021), https://doi.org/10.5772/intechopen.100293.

[7] P. Simonis, T. Dufour, H. Tenenbaum, Long-term implant survival and success: a 10–16-year follow-up of non-submerged dental implants: Long-term implant survival and success, Clin. Oral Implants Res. 21 (2010) 772–777, https://doi.org/10.1111/j.1600-0501.2010.01912.x.

[8] L.A. Damiati, M.P. Tsimbouri, V.-L. Hernandez, V. Jayawarna, M. Ginty, P. Childs, Y. Xiao, K. Burgess, J. Wells, M.R. Sprott, R.M.D. Meek, P. Li, R.O.C. Oreffo, A. Nobbs, G. Ramage, B.o. Su, M. Salmeron-Sanchez, M.J. Dalby, Materials-driven fibronectin assembly on nanoscale topography enhances mesenchymal stem cell adhesion, protecting cells from bacterial virulence factors and preventing biofilm formation, Biomaterials 280 (2022) 121263, https://doi.org/10.1016/j.biomaterials.2021.121263.

[9] B. Aslam, W. Wang, M.I. Arshad, M. Khurshid, S. Muzammil, M.H. Rasool, M. A. Nisar, R.F. Alvi, M.A. Aslam, M.U. Qamar, M.K.F. Salamat, Z. Baloch, Antibiotic resistance: a rundown of a global crisis, Infect. Drug Resist. 11 (2018) 1645–1658, https://doi.org/10.2147/IDR.S173867.

[10] W. Teughels, N. Van Assche, I. Sliepen, M. Quirynen, Effect of material characteristics and/or surface topography on biofilm development, Clin. Oral Implants Res. 17 (S2) (2006) 68–81, https://doi.org/10.1111/j.1600-0501.2006.01353.x.

[11] N. Epperlein, F. Menzel, K. Schwibbert, R. Koter, J. Bonse, J. Sameith, J. Krüger, J. Toepel, Influence of femtosecond laser produced nanostructures on biofilm growth on steel, Appl. Surf. Sci. 418 (2017) 420–424, https://doi.org/10.1016/j.apsusc.2017.02.174.

[12] X. Luo, S. Yao, H. Zhang, M. Cai, W. Liu, R. Pan, C. Chen, X. Wang, L. Wang, M. Zhong, Biocompatible nano-ripples structured surfaces induced by femtosecond laser to rebel bacterial colonization and biofilm formation, Opt. Laser Technol. 124 (2020) 105973, https://doi.org/10.1016/j.optlastec.2019.105973.

[13] K. Doll, E. Fadeeva, J. Schaeske, T. Ehmke, A. Winkel, A. Heisterkamp, B. N. Chichkov, M. Stiesch, N.S. Stumpp, Development of Laser-Structured Liquid-Infused Titanium with Strong Biofilm-Repellent Properties, ACS Appl. Mater. Interfaces. 9 (11) (2017) 9359–9368, https://doi.org/10.1021/acsami.6b16159.

[14] A.H.A. Lutey, L. Gemini, L. Romoli, G. Lazzini, F. Fuso, M. Faucon, R. Kling, Towards Laser-Textured Antibacterial Surfaces, Sci. Rep. 8 (2018) 10112, https://doi.org/10.1038/s41598-018-28454-2.

[15] V. Dumas, A. Rattner, L. Vico, E. Audouard, J.C. Dumas, P. Naisson, P. Bertrand, Multiscale grooved titanium processed with femtosecond laser influences mesenchymal stem cell morphology, adhesion, and matrix organization, J. Biomed. Mater. Res. A 100A (11) (2012) 3108–3116, https://doi.org/10.1002/jbm.a.34239.

[16] A. Cunha, O.F. Zouani, L. Plawinski, A.M. Botelho do Rego, A. Almeida, R. Vilar, M.-C. Durrieu, Human mesenchymal stem cell behavior on femtosecond laser-textured Ti-6Al-4V surfaces, Nanomed. 10 (5) (2015) 725–739, https://doi.org/10.2217/nnm.15.19.

[17] M. Maalouf, A. Abou Khalil, Y. Di Maio, S. Papa, X. Sedao, E. Dalix, S. Peyroche, A. Guignandon, V. Dumas, Polarization of Femtosecond Laser for Titanium Alloy Nanopatterning Influences Osteoblastic Differentiation, Nanomaterials. 12 (2022) 1619. https://doi.org/10.3390/nano12101619.

[18] C. Florian, S.V. Kirner, J. Krüger, J. Bonse, Surface functionalization by laser-induced periodic surface structures, J. Laser Appl. 32 (2) (2020) 022063, https://doi.org/10.2351/7.0000103.

[19] A. San-Blas, M. Martinez-Calderon, J. Buencuerpo, L.M. Sanchez-Brea, J. del Hoyo, M. Gómez-Aranzadi, A. Rodríguez, S.M. Olaizola, Femtosecond laser fabrication of LIPSS-based waveplates on metallic surfaces, Appl. Surf. Sci. 520 (2020) 146328, https://doi.org/10.1016/j.apsusc.2020.146328.

[20] S.S. Socransky, Microbiology of periodontal disease – present status and future considerations, J. Periodontol. 48 (9) (1977) 497–504, https://doi.org/10.1902/jop.1977.48.9.497.

[21] A. Butera, M. Pascadopoli, M. Pellegrini, S. Gallo, P. Zampetti, A. Scribante, Oral Microbiota in Patients with Peri-Implant Disease: A Narrative Review, Appl. Sci. 12 (2022) 3250, https://doi.org/10.3390/app12073250.
[22] Y. Hao, X. Huang, X. Zhou, M. Li, B. Ren, X. Peng, L. Cheng, Influence of Dental Prosthesis and Restorative Materials Interface on Oral Biofilms, Int. J. Mol. Sci. 19 (2018) 3157, https://doi.org/10.3390/ijms19103157.
[23] S.E. Mountcastle, S.C. Cox, R.L. Sammons, S. Jabbari, R.M. Shelton, S.A. Kuehne, A review of co-culture models to study the oral microenvironment and disease, J. Oral Microbiol. 12 (1) (2020) 1773122, https://doi.org/10.1080/20002297.2020.1773122.
[24] S. Ivanovski, R. Lee, Comparison of peri-implant and periodontal marginal soft tissues in health and disease, Periodontol. 2000 (76) (2018) 116–130, https://doi.org/10.1111/prd.12150.
[25] T. Guo, K. Gulati, H. Arora, P. Han, B. Fournier, S. Ivanovski, Race to invade: Understanding soft tissue integration at the transmucosal region of titanium dental implants, Dent. Mater. Off. Publ. Acad. Dent. Mater. 37 (5) (2021) 816–831, https://doi.org/10.1016/j.dental.2021.02.005.
[26] M.Á. Pacha-Olivenza, R. Tejero, M.C. Fernández-Calderón, E. Anitua, M. Troya, M. L. González-Martín, Relevance of Topographic Parameters on the Adhesion and Proliferation of Human Gingival Fibroblasts and Oral Bacterial Strains, BioMed Res. Int. 2019 (2019) 1–13, https://doi.org/10.1155/2019/8456342.
[27] H. Noh, E.A. Vogler, Volumetric Interpretation of Protein Adsorption: Competition from Mixtures and the Vroman Effect, Biomaterials 28 (3) (2007) 405–422, https://doi.org/10.1016/j.biomaterials.2006.09.006.
[28] S.M. Oliveira, N.M. Alves, J.F. Mano, Cell interactions with superhydrophilic and superhydrophobic surfaces, J. Adhes. Sci. Technol. 28 (8-9) (2014) 843–863, https://doi.org/10.1080/01694243.2012.697776.
[29] O. Raimbault, S. Benayoun, K. Anselme, C. Mauclair, T. Bourgade, A.-M. Kietzig, P.-L. Girard-Lauriault, S. Valette, C. Donnet, The effects of femtosecond laser-textured Ti-6Al-4V on wettability and cell response, Mater. Sci. Eng. C 69 (2016) 311–320, https://doi.org/10.1016/j.msec.2016.06.072.
[30] A.-M. Kietzig, S.G. Hatzikiriakos, P. Englezos, Patterned Superhydrophobic Metallic Surfaces, Langmuir 25 (8) (2009) 4821–4827, https://doi.org/10.1021/la8037582.
[31] P. Segovia, A. Wong, R. Santillan, M. Camacho-Lopez, S. Camacho-Lopez, Multi-phase titanium oxide LIPSS formation under fs laser irradiation on titanium thin films in ambient air, Opt. Mater. Express. 11 (9) (2021) 2892, https://doi.org/10.1364/OME.431210.
[32] M. Prudent, D. Iabbaden, F. Bourquard, S. Reynaud, Y. Lefkir, A. Borroto, J.-F. Pierson, F. Garrelie, J.-P. Colombier, High-Density Nanowells Formation in Ultrafast Laser-Irradiated Thin Film Metallic Glass, Nano-Micro Lett. 14 (2022) 103, https://doi.org/10.1007/s40820-022-00850-4.
[33] C. Florian, D. Fischer, K. Freiberg, M. Duwe, M. Sahre, S. Schneider, A. Hertwig, J. Krüger, M. Rettenmayr, U. Beck, A. Undisz, J. Bonse, Single Femtosecond Laser-Pulse-Induced Superficial Amorphization and Re-Crystallization of Silicon, Materials. 14 (2021) 1651, https://doi.org/10.3390/ma14071651.
[34] V. Dumas, A. Guignandon, L. Vico, C. Mauclair, X. Zapata, M.T. Linossier, W. Bouleftour, J. Granier, S. Peyroche, J.-C. Dumas, H. Zahouani, A. Rattner, Femtosecond laser nano/micro patterning of titanium influences mesenchymal stem cell adhesion and commitment, Biomed. Mater. 10 (5) (2015) 055002, https://doi.org/10.1088/1748-6041/10/5/055002.
[35] A. Klos, X. Sedao, T.E. Itina, C. Helfenstein-Didier, C. Donnet, S. Peyroche, L. Vico, A. Guignandon, V. Dumas, Ultrafast Laser Processing of Nanostructured Patterns for the Control of Cell Adhesion and Migration on Titanium Alloy, Nanomaterials. 10 (2020) 864, https://doi.org/10.3390/nano10050864.
[36] S. Hsiao, A. Crow, W. Lam, C. Bertozzi, D. Fletcher, M. Francis, DNA-coated AFM cantilevers for the investigation of cell adhesion and the patterning of live cells, Angew. Chem. Int. Ed Engl. 47 (44) (2008) 8473–8477, https://doi.org/10.1002/anie.200802525.
[37] A. Sancho, I. Vandersmissen, S. Craps, A. Luttun, J. Groll, A new strategy to measure intercellular adhesion forces in mature cell-cell contacts, Sci. Rep. 7 (2017) 46152, https://doi.org/10.1038/srep46152.
[38] A. Ahmad Khalili, M.R. Ahmad, A Review of Cell Adhesion Studies for Biomedical and Biological Applications, Int. J. Mol. Sci. 16 (2015) 18149–18184, https://doi.org/10.3390/ijms160818149.
[39] D.W. Zhou, A.J. García, Measurement Systems for Cell Adhesive Forces, J. Biomech. Eng. 137 (2015) 0209081–0209088, https://doi.org/10.1115/1.4029210.
[40] E. Babaliari, P. Kavatzikidou, D. Angelaki, L. Chaniotaki, A. Manousaki, A. Siakouli-Galanopoulou, A. Ranella, E. Stratakis, Engineering Cell Adhesion and Orientation via Ultrafast Laser Fabricated Microstructured Substrates, Int. J. Mol. Sci. 19 (2018) 2053, https://doi.org/10.3390/ijms19072053.
[41] S.W. Lee, K.S. Phillips, H. Gu, M. Kazemzadeh-Narbat, D. Ren, How microbes read the map: Effects of implant topography on bacterial adhesion and biofilm formation, Biomaterials 268 (2021) 120595, https://doi.org/10.1016/j.biomaterials.2020.120595.
[42] Y. Cheng, G. Feng, C.I. Moraru, Micro- and Nanotopography Sensitive Bacterial Attachment Mechanisms: A Review, Front. Microbiol. 10 (2019). https://www.frontiersin.org/article/10.3389/fmicb.2019.00191 (accessed June 22, 2022).
[43] D.P. Linklater, V.A. Baulin, S. Juodkazis, R.J. Crawford, P. Stoodley, E.P. Ivanova, Mechano-bactericidal actions of nanostructured surfaces, Nat. Rev. Microbiol. 19 (1) (2021) 8–22, https://doi.org/10.1038/s41579-020-0414-z.
[44] N.A. Yahaya, N. Yamada, Y. Kotaki, T. Nakayama, Characterization of light absorption in thin-film silicon with periodic nanohole arrays, Opt. Express. 21 (2013) 5924–5930, https://doi.org/10.1364/OE.21.005924.
[45] G. Lazzini, L. Romoli, A.H.A. Lutey, F. Fuso, Modelling the interaction between bacterial cells and laser-textured surfaces, Surf. Coat. Technol. 375 (2019) 8–14, https://doi.org/10.1016/j.surfcoat.2019.06.078.
[46] A. Nakhoul, C. Maurice, M. Agoyan, A. Rudenko, F. Garrelie, F. Pigeon, J.-P. Colombier, Self-Organization Regimes Induced by Ultrafast Laser on Surfaces in the Tens of Nanometer Scales, Nanomater. Basel Switz. 11 (2021) 1020, https://doi.org/10.3390/nano11041020.